Discovery of Mount Mazama cryptotephra in Lake Superior (North America): Implications and potential applications

N.G. Spano[1]*[†], C.S. Lane[2]*, S.W. Francis[3]*, and T.C. Johnson[1,4]*

[1]Large Lakes Observatory and Department of Earth and Environmental Sciences, University of Minnesota-Duluth, Duluth, Minnesota 55812, USA

[2]Department of Geography, University of Cambridge, Downing Place, Cambridge CB2 3EN, UK

[3]Department of Geology, Oberlin College, Oberlin, Ohio 44074, USA

[4]Department of Geosciences, University of Massachusetts, Amherst, Massachusetts 01003, USA

*E-mails: spano@berkeley.edu; csl44@cam.ac.uk; sarahf.619@gmail.com; tcj@d.umn.edu

[†]Current address: Department of Integrative Biology and Museum of Paleontology, University of California–Berkeley, Berkeley, California 94720, USA.

ABSTRACT

Tephrochronology is a widely applied method recognized for its exceptional precision in geologic dating and stratigraphic correlation. Tephra from the ~7.6 kyr B.P. Mount Mazama caldera-forming (”climactic”) eruption have been widely identified and applied as stratigraphic isochrons sediments of northwestern North America, as well as in the Greenland ice core records. Recent findings of a microscopic tephra accumulation, or cryptotephra, from Mazama in Newfoundland indicated that this horizon should also be

found in Lake Superior sediments. We present findings that confirm the presence of Mazama ash in two sediment cores from the Lake Superior basin, which indicates its likely presence in the rest of the Laurentian Great Lakes and in deposits throughout much of eastern North America and beyond. The ubiquity of this stratigraphic horizon should be applicable to a higher resolution evaluation of climatological, ecological, and archaeological events during the early- to mid-Holocene thermal maximum throughout much of North America.

INTRODUCTION

The summit of Mount Mazama (Crater Lake, Oregon, 42.95°N, 122.10°W) collapsed in a series of pyroclastic eruptions at 7682–7584 cal. yr B.P. (Egan et al., 2015). The eruptions released ~50 km^3 of dominantly low-silica rhyolitic magma and created the Crater Lake caldera (Bacon and Lanphere, 2006). The Plinian eruption cloud from this caldera-forming ("climactic") eruption is estimated to have risen to ~50 km, well into the stratosphere (Young, 1990) leaving deposits across the Pacific Northwest of North America that have been studied for their archaeologic, volcanic, environmental, and stratigraphic implications (e.g. Pyne-O'Donnell et al., 2012; Sarna-Wojcicki et al., 1983). While the majority of these studies targeted macroscopically visible Mazama tephra horizons , recent advances in distal tephrochronology have highlighted the stratigraphic value of cryptotephra: horizons too fine-grained, or in too low concentration, to be seen with the naked eye (Lowe and Hunt, 2001). In this form, Mazama ash has been found as far afield as Newfoundland (Pyne-O'Donnell et al., 2012) and Greenland (Zdanowicz et al., 1999) and therefore must have been deposited widely across the North American continent. Widespread discovery of the Mazama ash as a cryptotephra isochron, as illustrated by this study of the Lake Superior Basin, provides opportunities for stratigraphic correlation unsurpassed by other stratigraphic proxies, for precise correlation of sedimentary archives across the North American continent.

Isochrons are much needed, in part, because of the limitations of other dating methods like radiocarbon. In the Lake Superior basin, biogenic carbonates are not preserved in the lake sediment, and there is a large and varying proportion of old, re-suspended organic carbon that gets reworked into sediments that accumulate in the deep basins offshore (Zigah et al., 2014). Consequently, the primary approach to dating sediment cores from Lake Superior has been to measure the paleomagnetic secular variation (psv) in inclination and declination of the sediment and compare the resultant profiles to the magnetic field history established in well-dated cores from smaller lakes in the region (e.g., Breckenridge et al., 2004). Uncertainty arises in this approach of "wiggle matching", which can be alleviated by accurately ascertaining the age of independently dated horizons in the sediment sequence. One such chronostratigraphic approach is tephrochronology, which, to this point, had not been applied to Holocene sediment sequences in the Laurentian Great Lakes. Tephra from the ~7.6 kyr B.P. Mazama eruption offer a precisely dated isochron for checking the psv chronologies for the Lake Superior sediments during the Holocene thermal maximum (HTM). Here we present our discovery of Mazama cryptotephra in two sediment cores from Lake Superior (Fig. 1).

METHODS

Two piston cores were recovered from Lake Superior in 2009 and 2011. In 2009 the "KB core" was recovered in Keweenaw Bay (47.13°N, 87.82°W) in 127 m water depth (BH09K-1A-1K, International Geo Sample Number [IGSN]: IESUP0001) and in

2011 the "IR core" was recovered from near Isle Royale (47.97°N, 88.47°W) at a water depth of 233 m (BH11IR-SUP11–1A-1P, IGSN: IESUP0002) . PSV age models were developed for both cores using psv profiles and considering the transition depth in each core from glacial-lacustrine varves to post-glacial, more homogeneous sediment (O'Beirne, 2013). We determined from these age models that the Mazama cryptotephra, if present, would be found within 3.5–5.0 m below lake floor (mblf) in the core KB and 2.6–3.5 mblf in the core IR (Fig. 2).

We detected and extracted cryptotephra using the physical separation methods outlined in Blockley et al. (2005). Contiguous 10 cm sediment samples (~3 g wet weight) were extracted over the targeted intervals of each core. The samples were suspended in distilled water, disaggregated with a sonic dismembrator, and then digested in a 35% hydrogen peroxide solution at ~30 °C overnight. The cooled samples were each sieved through 25 μm meshes. Density separation of the >25 μm sediments utilized sodium polytungstate (SPT) to isolate sediments between 2.10 g cm^{-3} and 2.55 g cm^{-3}. This density range was experimentally determined in this study as optimal for separating both less-dense diatoms and more-dense silicate minerals from the tephra grains. We routinely prepared slides of sample blanks (centrifuged aliquots of the SPT solution) in order to check for any contamination during laboratory processing.

Each extracted sample was examined for tephra glass shards using a polarizing microscope. Shard counts were normalized by the original sample wet mass to determine the concentration of shards per gram (s/g) . The 10 cm increments found to have the highest concentrations were subsampled and processed again at a 1 cm interval to further resolve the depth of each cryptotephra horizon (Table DR1 in the GSA Data

Repository[1]). A homogenized portion of the subsample containing the highest concentration of shards from each core was examined by scanning-electron microscope (SEM) and another homogenized portion was mounted in a 25 mm epoxy resin block, which was then sectioned and polished for electron microprobe analysis, using wavelength dispersive spectrometry (WDS-EMPA) at the Research Laboratory for Archaeology and the History of Art, University of Oxford (UK). Eleven major- and minor-element oxides were measured on 24 tephra shards across the two sites (KB, n = 6; IR, n = 18), with intermittent analysis of secondary glass standards in order to monitor instrumental accuracy and analytical precision (Table DR2). Microprobe analytical conditions followed protocols established by the International focus group on Tephrochronology and Volcanism (INTAV; Kuehn et al., 2011; Table DR2).

Glass shard compositions were compared to compatible tephra glass shard data sets from Holocene rhyolitic eruptions in northwestern North America (Carson et al., 2002; Pyne-O’Donnell et al., 2012; Foit and Mehringer, 2016) (Fig. 4) and the Kamchatka Peninsula of Russia (Kyle et al., 2011), that are either known to be extremely widespread, or that occurred within a 2000 yr time window around the Mazama eruption (~9500–5500 yr B.P.).

RESULTS

We found significant amounts of tephra glass shards in each core of this study. The average background concentration of shards in the KB core was ~10 shards per gram (s/g) of 10 cm targeted sample and ~70 s/g of 1 cm targeted subsample (Fig. 3). The average background concentration in the IR core was ~2 s/g of 10 cm targeted sample and ~60 s/g of 1 cm targeted subsample. Shard concentrations were orders of magnitude higher in the sediment intervals identified as tephra horizons. Ambiguous grains (e.g., grains that could resemble phytoliths or tephra) were minor, but when present, were not counted as tephra shards. We use the difference in tephra shard concentrations above background values to define each horizon, rather than the absolute number of shards alone. No tephra shards were found in our blank samples; therefore, we interpret the background tephra levels as a real contribution from the catchment or sediment sources upwind from Lake Superior.

We identified one distinct horizon in the IR core at a depth of 2.914–2.924 mblf (Fig. 3; Table DR1). In this layer, shard concentrations reached a maximum of 3760 s/g (Fig. 3). We identified a more widely distributed horizon in KB at a depth of 4.40–4.44 mblf (Fig. 3; Table DR1). The concentration in this horizon rose to 500 s/g, which is not as enriched above background concentrations as the more focused horizon in the IR core (Fig. 3). However the integrated number of shards over the sampled 1 cm^{-2} area was of the same order of magnitude, ~2000 to 4000 cm^{-2}, in both cores (Fig. 3).

The cryptotephra shards observed in the KB and IR cores are dominantly fluted and pumiceous with a minor number of cuspate shards (Fig. 4). Fluted shards were typically ~75 μm long by ~30 μm wide. Sub-rounded, pumiceous shards were generally ~25 μm in diameter. Sub-angular, cuspate shards were up to ~40 μm in diameter. The largest shards found were ~125 μm long. These observed sizes may represent a distribution systematically skewed to a coarser size by our use of a 25 μm sieve. The shard morphotypes are similar to those of both proximal and distal Mazama ash from other studies (e.g., Enache and Cumming, 2006; Zdanowicz et al., 1999).

Correlation of element oxide concentrations from the KB and IR core tephra layers confirms that they represent the same low-silica rhyolitic horizon (Fig. 4), composed of 73 ± 0.7 wt% SiO_2, 14.22 ± 1.2 wt% Al_2O_3, 1.5 ± 0.1 wt% CaO, 4.8 ± 0.2 wt% NaO_2, and 3 ± 0.1 wt% K_2O (mean values ± two standard deviations). Tephra from the Mount Mazama climactic eruption and the Llao Rock precursor (Foit and Mehringer, 2016) event are the closest compositional matches to our Lake Superior tephra horizons. The Llao Rock tephra can be distinguished by a ~0.3 wt% difference in FeO content (Llao Rock wt% FeO ≈2.18; Lake Superior wt% FeO ≈1.87) (Table DR2; Fig. 4). Compositions of other major early- to mid-Holocene eruption sources from northwestern North America (Carson et al., 2002; Pyne-O'Donnell et al., 2012) do not match our results, confirming that Mazama tephra offer the only possible correlations (Table DR2; Fig. 4). Although work by Pearce et al. (2011) has shown that trace elements can also be useful for geochemical identification of cryptotephra, these data currently do not yet exist for Mazama ash records and are not required to confirm the major and minor element correlation.

Many explosive eruptions can generate tephra deposits that are dispersed over intercontinental distances (Lane et al., 2017), so it is conceivable that rhyolitic tephra from eruptions in the Kamchatka Peninsula of northeastern Russia and southwestern Alaska could reach Lake Superior (Mackay et al., 2016). However, there are no compositional matches for our KB and IR tephra in datasets of Kamchatka (Kyle et al., 2011) or southwestern Alaskan tephra (Carson et al., 2002). Our Lake Superior tephra shows a match only to tephra from the climactic eruption of Mount Mazama.

DISCUSSION AND CONCLUSIONS

The segments of both the KB and IR cores that we examined in this study consist of brown homogenous muds. The difference in burial depths of the cryptotephra (KB core cryptotephra horizon = 4.42 mblf; IR core cryptotephra horizon = 2.92 mblf) simply reflects a faster sedimentation rate in Keweenaw Bay compared to that in the deep basin off Isle Royale (Fig. 1B). We attribute the more dispersed distribution of tephra in the KB core than in the IR core to more intense biological mixing of the sediment by benthic organisms in Keweenaw Bay, where the density of benthic organisms is likely greater than that in the deep basins of the open lake (Heuschele, 1982).

The Mazama Llao Rock tephra were erupted between 7955 and 7610 cal yr B.P. (calibrated from Foit and Mehringer, 2016), and are considered a precursor to the climactic eruption of Mount Mazama at 7682–7584 cal yr B.P. (Egan et al., 2015). Despite a number of studies investigating the impact and occurrence of Holocene Mazama tephra on lacustrine systems in western North America (e.g., Adam et al., 1989; Starratt et al., 2003; Egan et al., 2016), the Llao Rock tephra has not previously been observed far to the east of the Cascades. The occurrence of a single and high-concentration peak of tephra shards in both of our cores from Lake Superior leads us to conclude that our tephra layer correlates to the more voluminous and more powerful climactic eruption of Mount Mazama and that the Llao Rock precursor event either did not make it this far across the continent, or is not detectable above a background high abundance of climactic Mazama shards.

The position of the Mazama climactic eruption in the IR and KB cores from Lake Superior appears to verify the less precise psv age assignment at ca. 8000–7500 yr B.P. (Fig. 2). The combination of geochemistry, age relations, and the location of this site within the expected distribution area that all support identification of the tephra as belonging to the Mazama climactic deposit. Our results indicate the potential of further cryptotephra analyses in verifying existing chronologies for sediment cores from Lake Superior, as well as other key paleoenvironmental archives where age-modeling has been found challenging. At present, our detection of the Mazama cryptotephra in Lake Superior, coupled with its discovery in Newfoundland (Pyne-O'Donnell et al., 2012), implies that this important stratigraphic horizon and potentially others can be found in other basins throughout North America. This offers an opportunity for improving the temporal accuracy in studies addressing the climate, sedimentology, ecology, and archaeology of the early- to mid-Holocene. In particular, the climactic Mazama eruption occurred during the HTM, when temperatures in North America were ~2.5–5.0 °C warmer than preindustrial levels (Renssen et al., 2012).

With measurable quantities of the Mazama cryptotephra present across much of North America, feedbacks between climate and vegetation, and environments of human occupation can be investigated at more precise spatial and temporal scales. The impact of the HTM in North America was spatially variable, with temperature anomalies ranging from 1 to 6 °C across the Northern Hemisphere (Renssen et al., 2012). The precisely-dated Mazama tephra horizon could serve as the key stratigraphic marker for a synoptic study of the HTM across a broad swath of the North American continent (and beyond, including North Atlantic marine sediments and European lakes and peatlands) (e.g., Pyne-O'Donnell et al., 2016) at a time of unusual warmth and aridity, perhaps not unlike what we will face in the coming decades of this century.

ACKNOWLEDGMENTS

We thank the crew of the R/V *Blue Heron* for their invaluable assistance in recovering the piston cores from Lake Superior, and colleagues at LacCore, the National Lake Core Repository at the University of Minnesota–Twin Cities (USA) campus for archiving the cores and their guidance in core sampling. Spano and Francis thank Benjamin Chorn for initial cryptotephra training, and Bryan Bandli in the University of Minnesota–Duluth Department of Earth and Environmental Sciences for training in SEM and EMPA preparation. We thank Victoria Smith at the Research Laboratory for Archaeology and the History of Art, University of Oxford (UK), for electron microprobe analyses. This research was supported by a Regents Professor grant by the University of Minnesota to Johnson.

REFERENCES CITED

Adam, D.P., Sarna-Wojcicki, A.M., Rieck, H.J., Bradbury, J.P., Dean, W.E., and Forester, R.M., 1989, Tulelake, California: The last 3 million years: Palaeogeography, Palaeoclimatology, Palaeoecology, v. 72, p. 89–103, doi:https://doi.org/10.1016/0031-0182(89)90134-X.

Bacon, C.R., 1983, Eruptive history of Mount Mazama and Crater Lake caldera, Cascade Range, USA: Journal of Volcanology and Geothermal Research, v. 18, p. 57–115, doi:https://doi.org/10.1016/0377-0273(83)90004-5.

Bacon, C.R., and Lanphere, M.A., 2006, Eruptive history and geochronology of Mount Mazama and the Crater Lake region, Oregon: Geological Society of America Bulletin, v. 118, p. 1331–1359, doi:https://doi.org/10.1130/B25906.1.

Blockley, S.P.E., Pyne-O'Donnell, S.D.F., Lowe, J.J., Matthews, I.P., Stone, A., Pollard, A.M., Turney, C.S.M., and Molyneux, E.G., 2005, A new and less destructive laboratory procedure for the physical separation of distal glass tephra shards from sediments: Quaternary Science Reviews, v. 24, p. 1952–1960, doi:https://doi.org/10.1016/j.quascirev.2004.12.008.

Breckenridge, A., Johnson, T.C., Beske-Diehl, S., and Mothersill, J.S., 2004, The timing of regional Lateglacial events and post-glacial sedimentation rates from Lake Superior: Quaternary Science Reviews, v. 23, p. 2355–2367, doi:https://doi.org/10.1016/j.quascirev.2004.04.007.

Carson, E.C., Fournelle, J.H., Miller, T.P., and Mickelson, D.M., 2002, Holocene tephrochronology of the Cold Bay area, southwest Alaska Peninsula: Quaternary Science Reviews, v. 21, p. 2213–2228, doi:https://doi.org/10.1016/S0277-3791(02)00023-9.

Egan, J., Staff, R., and Blackford, J., 2015, A high-precision age estimate of the Holocene Plinian eruption of Mount Mazama, Oregon, USA: The Holocene, v. 25, p. 1054–1067, doi:https://doi.org/10.1177/0959683615576230.

Egan, J., Fletcher, W.J., Allott, T.E.H., Lane, C.S., Blackford, J.J., and Clark, D.T., 2016, The impact and significance of tephra deposition on a Holocene forest environment in the North Cascades, Washington, USA: Quaternary Science Reviews, v. 137, p. 135–155, doi:https://doi.org/10.1016/j.quascirev.2016.02.013.

Enache, M.D., and Cumming, B.F., 2006, The morphological and optical properties of volcanic glass: A tool to assess density-induced vertical migration of tephra in sediment cores: Journal of Paleolimnology, v. 35, p. 661–667, doi:https://doi.org/10.1007/s10933-005-3604-9.

Foit, F.F., and Mehringer, P.J., 2016, Holocene tephra stratigraphy in four lakes in southeastern Oregon and northwestern Nevada, USA: Quaternary Research, v. 85, p. 218–226, doi:https://doi.org/10.1016/j.yqres.2015.12.008.

Heuschele, A., 1982, Vertical distribution of profundai benthos in Lake Superior sediments: Journal of Great Lakes Research, v. 8, p. 603–613, doi:https://doi.org/10.1016/S0380-1330(82)71999-9.

Kuehn, S.C., Froese, D.G., Shane, P.A.R., and Participants, I.I., 2011, The INTAV intercomparison of electron-beam microanalysis of glass by tephrochronology laboratories: Results and recommendations: Quaternary International, v. 246, p. 19–47, doi:https://doi.org/10.1016/j.quaint.2011.08.022.

Kyle, P.R., Ponomareva, V.V., and Rourke Schluep, R., 2011, Geochemical characterization of marker tephra layers from major Holocene eruptions, Kamchatka Peninsula, Russia: International Geology Review, v. 53, p. 1059–1097, doi:https://doi.org/10.1080/00206810903442162.

Lane, C.S., Lowe, D.J., Blockley, S.P.E., Suzuki, T., and Smith, V.C., 2017, Advancing tephrochronology as a global dating tool: Applications in volcanology, archaeology, and palaeoclimatic research. Quaternary Geochronology, v. 40, p. 1-7, doi:http://dx.doi.org/10/1016/j.quageo.2017.04.003.

Lowe, D.J., and Hunt, J.B., 2001, A summary of terminology used in tephra-related studies, *in* Juvigne, E., and Raynal, J.P., eds., Tephras: Chronology, Archeology: Les dossiers de l'Archéo-Logis, v. l, p. 18–22.

Mackay, H., Hughes, P.D., Jensen, B.J., Langdon, P.G., Pyne-O'Donnell, S.D., Plunkett, G., Froese, D.G., Coulter, S., and Gardner, J.E., 2016, A mid to late Holocene cryptotephra framework from eastern North America: Quaternary Science Reviews, v. 132, p. 101–113, doi:https://doi.org/10.1016/j.quascirev.2015.11.011.

O'Beirne, M.D., 2013, A 10,000-Year Sedimentary Organic Geochemical Record of Lake Superior [M.S. thesis]: Duluth, Minnesota, University of Minnesota, 53 p.

Pearce, N.J.G., Perkins, W.T., Westgate, J.A., and Wade, S.C., 2011, Trace-element microanalysis by LA-ICP-MS: The quest for comprehensive chemical characterisation of single, sub-10 µm volcanic glass shards: Quaternary International, v. 246, p. 57–81, doi:https://doi.org/10.1016/j.quaint.2011.07.012.

Pyne-O'Donnell, S.D.F., et al., 2012, High-precision ultra-distal Holocene tephrochronology in North America: Quaternary Science Reviews, v. 52, p. 6–11, doi:https://doi.org/10.1016/j.quascirev.2012.07.024.

Pyne-O'Donnell, S.D.F., Cwynar, L.C., Jensen, B.J.L., Vincent, J.H., Kuehn, S.C., Spear, R., and Froese, D.G., 2016, West Coast volcanic ashes provide a new continental-scale Late glacial isochron: Quaternary Science Reviews, v. 142, p. 16–25, doi:https://doi.org/10.1016/j.quascirev.2016.04.014.

Renssen, H., Seppä, H., Crosta, X., Goosse, H., and Roche, D.M., 2012, Global characterization of the Holocene thermal maximum: Quaternary Science Reviews, v. 48, p. 7–19, doi:https://doi.org/10.1016/j.quascirev.2012.05.022.

Sarna-Wojcicki, A.M., Champion, D.E., and Davis, J.O., 1983, Holocene volcanism in the conterminous United States and the role of silicic volcanic ash layers in correlation of latest-Pleistocene and Holocene deposits, *in* Wright, H.E., Jr., ed., Late-Quaternary Environments of the United States: Minneapolis, Minnesota, University of Minnesota Press, p. 52–77.

Starratt, S.W., Barron, J.A., Kneeshaw, T., Phillips, R.L., Bischoff, J.L., Lowenstern, J.B., and Wanket, J.A., 2003, A Holocene record from Medicine Lake, Siskiyou County, California: Preliminary diatom, pollen, geochemical, and sedimentological data, *in* West, G.J., and Blomquist, N.L., eds., Proceedings of the Nineteenth Annual Pacific Climate Workshop, Technical Report 71 of the Interagency Ecological Program for the San Francisco Estuary, p. 131–148.

Young, S.R., 1990, Physical volcanology of Holocene airfall deposits from Mt. Mazama, Crater Lake, Oregon [Ph.D. thesis]: Lancaster, UK, University of Lancaster, 307 p.

Zdanowicz, C.M., Zielinski, G.A., and Germani, M.S., 1999, Mount Mazama eruption: Calendrical age verified and atmospheric impact assessed: Geology, v. 27, p. 621–624, doi:https://doi.org/10.1130/0091-7613(1999)027<0621:MMECAV>2.3.CO;2.

Zigah, P.K., Minor, E.C., Hussain, A.N.A., Werne, J.P., and Hatcher, P.G., 2014, An investigation of size-fractionated organic matter from Lake Superior and a tributary stream using radiocarbon, stable isotopes and NMR: Geochimica et Cosmochimica Acta, v. 127, p. 264–284, doi:https://doi.org/10.1016/j.gca.2013.11.037.

FIGURE CAPTIONS

Figure 1. Observed and inferred distribution of Mazama ash across North America and Greenland. Gray diamond depicts Nordan's Pond Bog in Newfoundland (Pyne-O'Donnell et al. (2012), asterisk depicts the Greenland Ice Sheet Project 2 (GISP2) (Zdanowicz et al., 1999). A: Areal distribution of readily visible Mazama ash in western North America (white shading; modified from Sarna-Wojcicki et al., 1983). B: Locations and depths of piston cores IR and in Lake Superior. Projection: WGS84.

Figure 2. Paleomagnetic inclination curves from the reference core LU83–8 (Breckenridge et al., 2004) in northern Lake Superior and cores KB (Keweenaw Bay) and IR (Isle Royale). Numbered inflection points mark stratigraphic correlations between cores (O'Beirne, 2013). Vertical black bars indicate the depths searched for cryptotephra and asterisks mark the tephra position. Horizontal bar on LU83–8 inclination graph corresponds to the modeled Mazama climactic eruption age of 7682– 7584 cal yr B.P. (Egan et al., 2015). Lighter gray shading represents glacial-lacustrine varves, which ceased to accumulate in Lake Superior ca. 9000 cal. yr B.P. (Breckenridge et al., 2004). Paleomagnetic analyses performed at LacCore, National Lake Core Repository (Minneapolis, Minnesota, USA).

Figure 3. Volcanic shard abundance versus depth (mblf) in Cores KB (Keweenaw Bay) and IR (Isle Royale). Light gray shading and upper x-axis refers to shard abundance per gram wet weight (Core KB) and shard counts (Core IR) in 10 cm increments down core. Dark bars and lower x-axis refers to 1 cm shard abundance within areas of highest tephra concentration.

Figure 4. A: Scanning electron microscope image of Mount Mazama tephra from Core IR (Isle Royale). Note the distinctive fluted and pumiceous glass shards. B: Bi-plots of glass shard compositions determined by WDS-EPMA on cryptotephra from Cores KB and IR, alongside published values for several tephra from western North America (Pyne-O'Donnell et al., 2012; Foit and Mehringer, 2016), with indicative envelopes for each volcanic region. There is good agreement between the compositions of tephra from Cores

KB and IR, and the reference Mazama ash (blue triangles vs. light green and yellow circles). Error bars (top-right) represent 2 standard deviations ($2CV_{std} \times \bar{x}_{Mazama\ ref}$). Full datasets provided in Table DR2 and are available online from the EarthChem data repository (http://dx.doi.org/10.1594/IEDA/100710).

[1]GSA Data Repository item 2017xxx, xxxxxxxx, is available online at http://www.geosociety.org/datarepository/2017/ or on request from editing@geosociety.org.

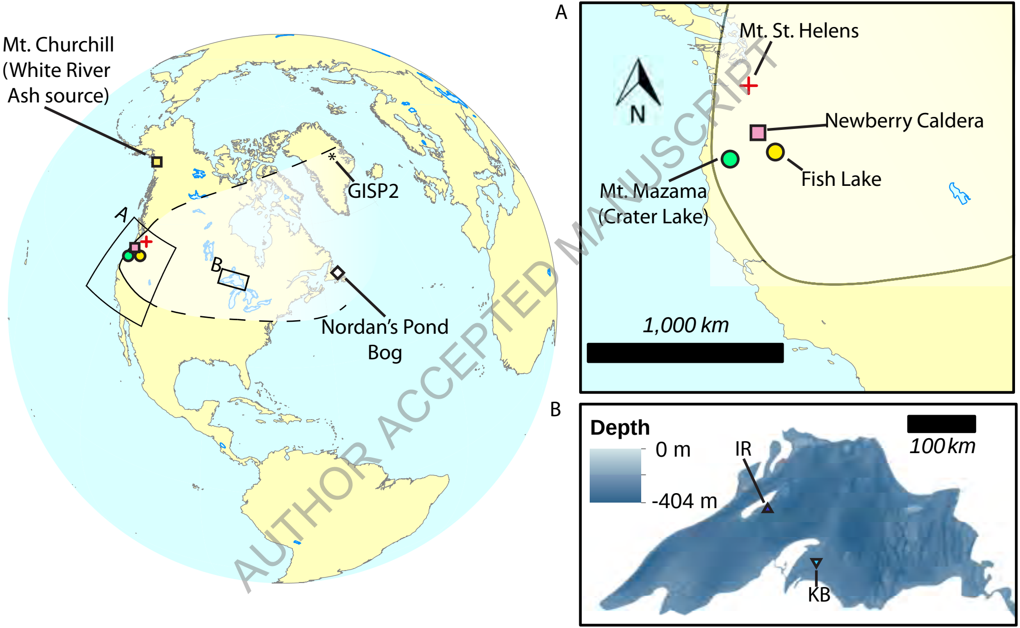
Mt. Churchill (White River Ash source)
GISP2
A
B
Nordan's Pond Bog
A
Mt. St. Helens
N
Newberry Caldera
Fish Lake
Mt. Mazama (Crater Lake)
1,000 km
B
Depth
0 m
-404 m
IR
KB
100 km

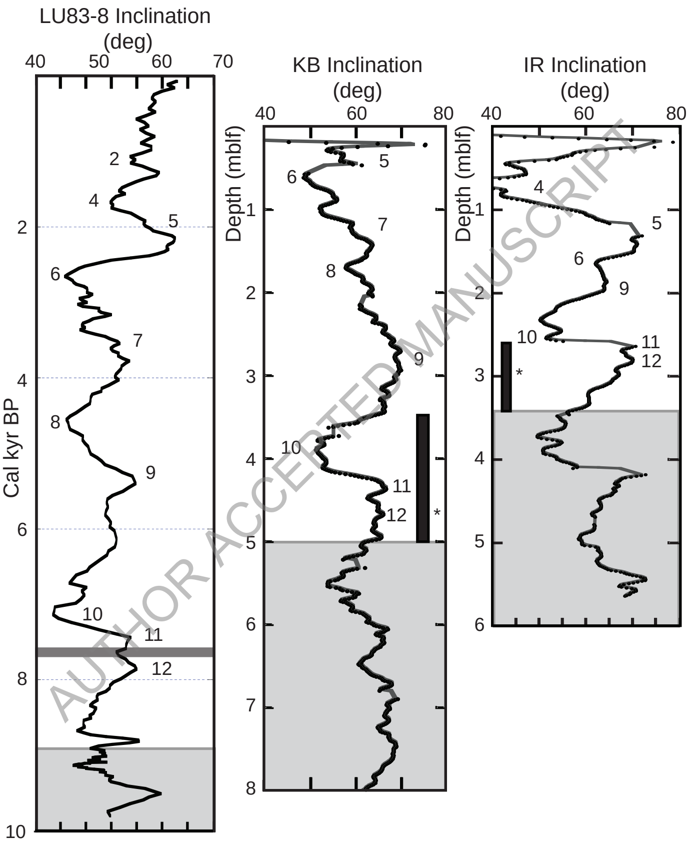

LU83-8 Inclination (deg)
KB Inclination (deg)
IR Inclination (deg)
Cal kyr BP
Depth (mblf)
Depth (mblf)
40
50
60
70
40
60
80
40
60
80
2
4
6
8
10
1
2
3
4
5
6
7
8
1
2
3
4
5
6
*
*

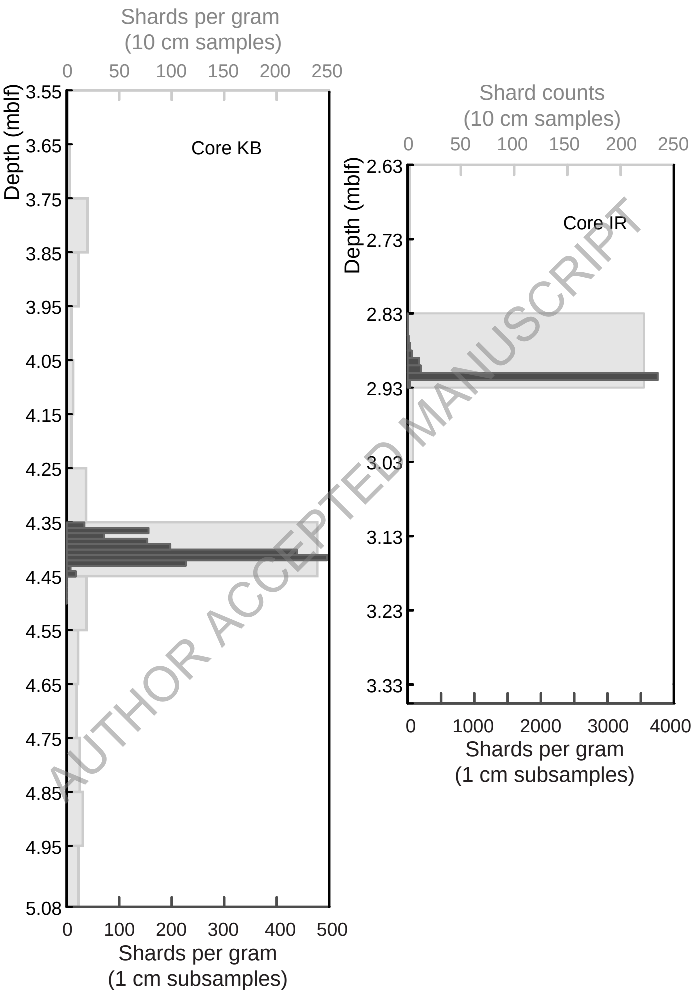
Shards per gram
(10 cm samples)
0
50
100
150
200
250
Depth (mblf)
3.55
3.65
3.75
3.85
3.95
4.05
4.15
4.25
4.35
4.45
4.55
4.65
4.75
4.85
4.95
5.08
Core KB
0
100
200
300
400
500
Shards per gram
(1 cm subsamples)
Shard counts
(10 cm samples)
0
50
100
150
200
250
Depth (mblf)
2.63
2.73
2.83
2.93
3.03
3.13
3.23
3.33
Core IR
0
1000
2000
3000
4000
Shards per gram
(1 cm subsamples)
AUTHOR ACCEPTED MANUSCRIPT

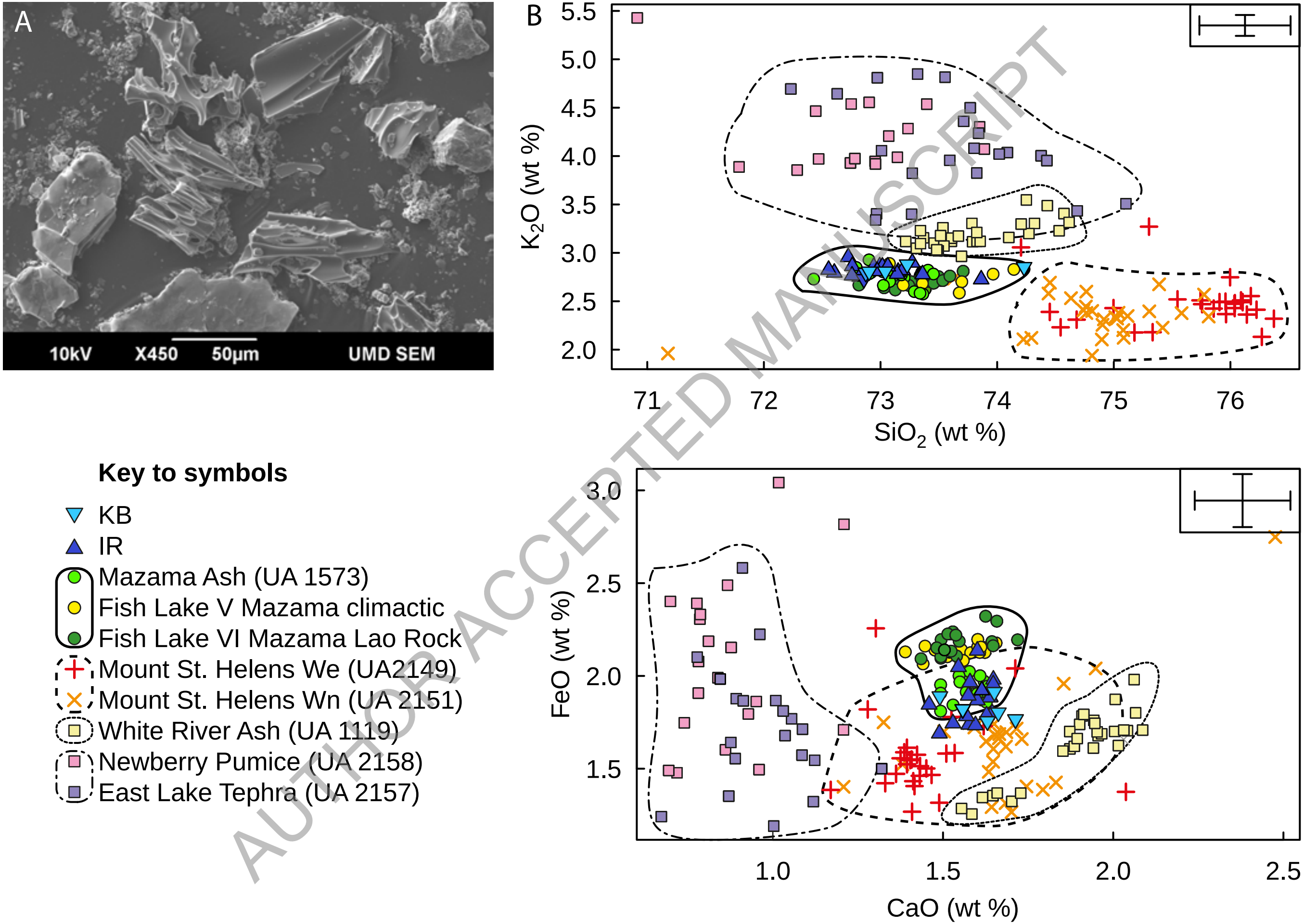
A
10kV
X450
50µm
UMD SEM
B
K2O (wt %)
SiO2 (wt %)
5.5
5.0
4.5
4.0
3.5
3.0
2.5
2.0
71
72
73
74
75
76
FeO (wt %)
CaO (wt %)
3.0
2.5
2.0
1.5
1.0
1.5
2.0
2.5
Key to symbols
KB
IR
Mazama Ash (UA 1573)
Fish Lake V Mazama climactic
Fish Lake VI Mazama Lao Rock
Mount St. Helens We (UA2149)
Mount St. Helens Wn (UA 2151)
White River Ash (UA 1119)
Newberry Pumice (UA 2158)
East Lake Tephra (UA 2157)

TABLE DR1. LAKE SUPERIOR SEDIMENT CORE SAMPLE DEPTHS AND CRYPTOTEPHRA SHARD CONCENTRATIONS

Site names, core sections, and sample names	Average depth of sample in core section (cm)	Average depth of sample, meters below lake floor (mblf)	Sample sediment mass (g)	Tephra shards (counts)	Tephra shard concentrations (counts g^{-1})
Keweenaw Bay (KB)					
BH09K-SUP09-1A-1K-4 (10 cm samples)					
LS 01	5	3.600	2.6447	3	1.1343
LS 02	15	3.700	1.4053	4	2.8463
LS 03	25	3.800	1.1099	22	19.821
LS 04	35	3.900	0.9645	11	11.404
LS 05	45	4.000	1.2741	6	4.7092
LS 06	55	4.100	1.1521	7	6.0758
LS 07	65	4.200	1.1103	5	4.5032
LS 08	75	4.300	1.4109	26	18.427
LS 09	85	4.400	0.8297	198	238.64
LS 10	95	4.500	1.2719	24	18.869
LS 11	105	4.600	0.9234	10	10.829
LS 12	115	4.700	1.1543	11	9.5295
LS 13	125	4.800	1.1986	15	12.514
LS 14	135	4.900	1.4921	23	15.414
LS 15	145	5.015	2.417	27	11.170
BH09K-SUP09-1A-1K-5 (10 cm samples)					
LS 16	5	5.19	0.7506	5	6.6613
LS 17	15	5.29	0.8451	8	9.4663
BH09K-SUP09-1A-1K-4 (1 cm subsamples)					
LS 18	80.50	4.355	0.8896	30	33.723
LS 19	81.50	4.365	0.8467	132	155.89
LS 20	82.50	4.375	1.1386	81	71.139
LS 21	83.50	4.385	0.9832	151	153.58
LS 22	84.50	4.395	1.1399	225	197.38
LS 23	85.50	4.405	1.4697	645	438.86
LS 24	86.50	4.415	1.7648	875	495.80
LS 25	87.50	4.425	1.5554	353	226.95
LS 26	88.50	4.435	1.3662	10	7.3195
LS 27	89.50	4.445	0.9802	17	17.343
Isle Royale (IR)					
BH11IR-SUP11-1A-1P-3 (10 cm samples)					
LS 31	5	2.679	N.D.*	2	N.D.*
LS 32	15	2.779	N.D.*	2	N.D.*
LS 33	25	2.879	N.D.*	222	N.D.*
LS 34	35	2.929	N.D.*	5	N.D.*
LS 35	45	3.079	N.D.*	1	N.D.*
LS 36	55	3.179	N.D.*	1	N.D.*
LS 37	65	3.279	N.D.*	0	N.D.*
BH11IR-SUP11-1A-1P-4 (10 cm samples)					
LS 38	107.5	5.239	N.D.*	0	N.D.*
LS 39	117.5	5.339	N.D.*	2	N.D.*
LS 40	127.5	5.439	N.D.*	3	N.D.*
BH11IR-SUP11-1A-1P-3 (1 cm subsamples)					
LS 41	20.50	2.834	1.5000	5	3.3333
LS 42	21.50	2.844	2.0000	5	2.5000

LS 43	22.50	2.854	2.8000	5	1.7857
LS 44	23.5	2.864	2.2	36	16.363
LS 45	24.5	2.874	2	79	39.500
LS 46	25.5	2.884	0.9	57	63.333
LS 47	26.5	2.894	0.7	119	170.00
LS 48	27.5	2.904	1.3	256	196.92
LS 49	28.5	2.914	1.5	5634	3756.0
LS 50	29.5	2.924	2	66	33.000

*N.D. = no data.

TABLE DR2. ELECTRON MICROPROBE ANALYSIS (EMPA) RESULTS*

	SiO_2	TiO_2	Al_2O_3	FeO	MnO	MgO	CaO	Na_2O	K_2O	Cl	P	Total
Keweenaw Bay (KB)												
LS 024 (IGSN: IESUP000U)												
	73.23	0.49	13.87	1.91	0.04	0.50	1.65	5.13	2.88	0.22	0.07	95.24
	73.04	0.45	14.35	1.80	0.09	0.42	1.66	5.10	2.81	0.23	0.05	99.16
	72.86	0.41	14.80	1.89	0.09	0.45	1.49	4.99	2.73	0.18	0.10	98.36
	72.87	0.44	14.58	1.75	0.08	0.47	1.63	5.14	2.79	0.18	0.07	99.79
	74.23	0.42	14.97	1.76	0.10	0.43	1.71	3.26	2.85	0.22	0.05	97.61
	72.90	0.40	14.80	1.82	0.04	0.42	1.56	4.99	2.81	0.21	0.06	98.05
Arithmetic mean	73.22	0.42	14.79	1.81	0.08	0.44	1.60	4.60	2.80	0.20	0.07	100.0
2SD	0.677	0.016	0.159	0.061	0.025	0.023	0.095	0.893	0.051	0.019	0.025	1.062
Isle Royale (IR)												
LS 049 (IGSN: IESUP001G)												
	73.00	0.43	14.25	1.88	0.04	0.45	1.64	5.18	2.83	0.22	0.08	97.59
	73.86	0.47	13.91	1.74	0.03	0.46	1.53	5.01	2.73	0.20	0.06	98.69
	72.60	0.48	14.48	1.98	0.01	0.46	1.65	5.19	2.80	0.25	0.10	99.87
	72.72	0.44	14.16	1.88	0.14	0.50	1.64	5.26	2.96	0.21	0.08	97.18
	72.55	0.41	14.27	2.05	0.07	0.47	1.55	5.53	2.83	0.20	0.09	98.72
	72.82	0.45	14.24	1.80	0.04	0.49	1.64	5.47	2.75	0.21	0.08	99.55
	73.36	0.42	14.20	1.84	0.00	0.43	1.46	5.21	2.78	0.23	0.07	97.76
	73.15	0.39	14.29	1.87	0.09	0.49	1.60	5.08	2.80	0.19	0.06	99.29
	73.19	0.47	14.25	1.69	0.11	0.45	1.49	5.25	2.82	0.21	0.07	98.89
	72.94	0.49	14.42	1.74	0.05	0.43	1.58	5.20	2.86	0.21	0.08	96.35
	73.27	0.43	14.08	1.96	0.06	0.48	1.58	4.95	2.90	0.21	0.08	95.68
	73.14	0.42	14.30	1.73	0.04	0.47	1.60	5.24	2.78	0.23	0.05	95.04
	72.99	0.48	14.40	1.78	0.00	0.43	1.57	5.18	2.86	0.23	0.07	97.11
	73.02	0.44	14.26	1.95	0.09	0.48	1.65	4.96	2.86	0.23	0.08	98.43
	72.76	0.47	14.54	1.89	0.07	0.44	1.57	5.12	2.86	0.23	0.04	96.24
	72.97	0.43	14.19	1.79	0.09	0.44	1.63	5.43	2.81	0.20	0.03	98.62
	73.06	0.47	14.15	2.13	0.00	0.46	1.60	4.95	2.86	0.22	0.09	96.35
	72.76	0.43	14.86	1.92	0.08	0.45	1.61	4.88	2.77	0.22	0.02	96.75
Arithmetic mean	72.89	0.45	14.44	1.93	0.06	0.45	1.60	5.09	2.83	0.22	0.05	100.0
2SD	0.155	0.024	0.330	0.146	0.040	0.011	0.023	0.243	0.046	0.014	0.030	2.047
Mazama Ash reference (Edmonton River valley), from Pyne-O'Donnell et al. (2012)												
UA 1573												
Arithmetic mean	73.12	0.41	14.40	1.93	0.07	0.44	1.58	5.15	2.74	0.19	N.D.†	97.4
2SD	0.573	0.067	0.312	0.116	0.055	0.070	0.097	0.305	0.200	0.059	N.D.†	3.16
Fish Lake V Mazama climactic reference, from Foit and Mehringer (2016)												
Arithmetic mean	73.38	0.421	14.25	2.132	N.D.†	0.491	1.547	4.882	2.726	0.167	N.D.†	98.55
2SD	0.573	0.036	0.294	0.064	N.D.†	0.055	0.148	0.245	0.134	0.10	N.D.†	2.39
Fish Lake VI Mazama Llao Rock reference, from Foit and Mehringer (2016)												
Arithmetic mean	73.28	0.398	14.47	2.183	N.D.†	0.463	1.552	4.781	2.71549	0.148	N.D.†	98.60
2SD	0.478	0.038	0.315	0.127	N.D.†	0.094	0.149	0.385	0.123	0.057	N.D.†	1.150
Mount St Helens We reference, from												

Pyne-O'Donnell et al. (2012)												
UA 2149												
Arithmetic mean	75.65	0.23	13.50	1.57	-0.01	0.28	1.45	4.76	2.47	0.11	N.D.†	98.74
2SD	1.240	0.23	0.982	0.43	0.20	0.26	0.31	0.44	0.49	0.06	N.D.†	2.220
Mount St Helens Wn reference, from Pyne-O'Donnell et al. (2012)												
UA 2151												
Arithmetic mean	74.78	0.21	13.99	1.65	0.02	0.33	1.69	4.88	2.35	0.09	N.D.†	96.94
2SD	1.694	0.30	0.989	0.56	0.33	0.29	0.45	0.57	0.41	0.07	N.D.†	4.24
White River Ash (eastern lobe) reference, from Pyne-O'Donnell et al. (2012)												
UA 1119												
Arithmetic mean	73.79	0.21	14.47	1.62	0.06	0.35	1.88	4.11	3.18	0.34	N.D.†	97.38
2SD	0.837	0.07	0.449	0.37	0.05	0.08	0.30	0.21	0.27	0.08	N.D.†	3.26
Newberry Pumice reference, from Pyne-O'Donnell et al. (2012)												
UA 2158												
Arithmetic mean	73.54	0.23	14.25	1.99	0.07	0.15	0.86	4.85	3.94	0.13	N.D.†	98.37
2SD	0.950	0.12	0.615	0.13	0.05	0.06	0.11	1.07	0.47	0.07	N.D.†	1.72
East Lake Tephra reference, from Pyne-O'Donnell et al. (2012)												
UA 2157												
Arithmetic mean	73.72	0.21	13.97	1.72	0.06	0.21	0.97	4.86	4.14	0.13	N.D.†	97.53
2SD	1.39	0.25	1.03	0.68	0.37	0.35	0.29	0.39	0.93	0.06	N.D.†	3.7
Kamchatka references, from Kyle et al. (2011)												
Kizimen volcano												
Arithmetic mean	77.07	0.24	12.75	1.31	0.03	0.24	1.59	3.48	3.04	0.16	0.03	100
2SD	0.6	0.08	0.5	0.12	0.06	0.18	0.12	N.D.†	0.18	0.04	0.06	1.94
Karymsky volcano												
Arithmetic mean	74.69	0.39	13.47	1.86	0.04	0.36	1.49	4.33	3.01	0.22	0.05	100
2SD	0.56	0.06	0.32	0.2	0.06	0.18	0.16	N.D.†	0.18	0.2	0.06	1.98
Avachinsky volcano												
Arithmetic mean	75.08	0.19	14.54	1.6	0.08	0.43	2.78	3.69	1.35	0.09	0.05	100
2SD	0.7	0.04	0.34	0.14	0.08	0.04	0.2	N.D.†	0.12	0.08	0.04	1.78
Ksudach volcano												
Arithmetic mean	70.37	0.64	14.61	4.35	0.16	0.87	3.05	4.3	1.24	0.14	0.15	100
2SD	0.84	0.06	0.44	0.34	0.1	0.1	0.22	N.D.†	0.1	0.06	0.06	2.32
Kurile Lake caldera												
Arithmetic mean	76.39	0.23	13.15	1.52	0.06	0.27	1.52	4.52	2.09	0.14	0.03	100
2SD	1.46	0.08	0.86	0.18	0.08	0.18	0.26	N.D.†	0.26	0.04	0.04	3.44
Southwestern Alaskan references, from Carson et al. (2002)												
Horizon A												
Arithmetic mean	57.30	1.88	15.28	9.79	0.23	2.79	5.69	4.21	1.65	N.D.†	N.D.†	99.66
2SD	2.02	0.32	1.88	1.76	0.24	1.22	1.02	1.27	0.52	N.D.†	N.D.†	1.25
Horizon B												
Arithmetic mean	77.22	0.11	13.58	1.69	0.13	0.15	1.41	4.11	1.55	N.D.†	N.D.†	100.00
2SD	1.38	0.12	0.68	0.26	0.10	0.06	0.42	0.78	0.30	N.D.†	N.D.†	0.00
Funk/Fisher ash 1												
Arithmetic mean	68.80	0.55	15.32	4.21	0.24	0.60	2.24	4.86	2.43	N.D.†	N.D.†	99.25

2SD	1.36	0.14	0.74	0.48	0.22	0.14	0.28	0.80	0.26	N.D.†	N.D.†	0.88
Funk/Fisher ash 2												
Arithmetic mean	68.87	0.56	15.37	4.24	0.19	0.62	2.34	4.73	2.41	N.D.†	N.D.†	99.33
2SD	1.04	0.12	0.54	0.58	0.12	0.14	0.24	0.66	0.22	N.D.†	N.D.†	0.88
Funk/Fisher ash 3												
Arithmetic mean	52.88	1.62	16.32	11.20	0.23	4.07	8.84	3.21	0.87	N.D.†	N.D.†	99.24
2SD	1.27	0.24	0.92	1.6	0.16	1.44	0.86	0.60	0.24	N.D.†	N.D.†	0.86
Funk/Fisher ash 4												
Arithmetic mean	69.15	0.60	15.44	4.38	0.18	0.64	2.39	4.20	2.39	N.D.†	N.D.†	99.37
2SD	1.96	0.66	0.44	0.60	0.16	0.22	0.96	0.72	0.18	N.D.†	N.D.†	0.46
ATHO-G standard												
Arithmetic mean	75.47	0.257	12.36	3.188	0.107	0.092	1.680	4.038	2.751	0.036	0.018	99.74
2SD	0.398	0.034	0.226	0.246	0.090	0.025	0.150	0.242	0.104	0.028	0.024	1.95
GOR132-G												
Arithmetic mean	46.36	0.287	11.16	10.24	0.132	22.45	8.48	0.794	0.041	0.008	0.039	98.21
2SD	0.173	0.073	0.180	0.392	0.099	0.339	0.177	0.077	0.023	0.018	0.030	1.61
StHs6/80-G standard												
Arithmetic mean	63.84	0.703	17.85	4.39	0.066	1.968	5.297	4.384	1.329	0.009	0.165	99.24
2SD	0.776	0.079	0.282	0.250	0.099	0.096	0.113	0.843	0.087	0.021	0.037	2.38

Microprobe operating conditions note:

EMPA for the Lake Superior samples and the fused volcanic glass standards ATHO-G, GOR132-G, and StHs6/80-G was conducted at the University of Oxford Research Laboratory for Archaeology and the History of Art with a JEOL JX8600 electron microprobe, in wavelength dispersive mode, with 15-keV accelerating voltage, 6-nA beam current, and a 10-µm defocused beam. On-peak count times were as follows: 10 s for Na; 30 s for Si, Al, K, Ca, Fe, Mg, Ti, and Mn; and 60 s for P. We applied a suite of characterized minerals and oxide standards to calibrate the electron probe while accuracy and precision were monitored by intermittent analysis of fused volcanic glass standards ATHO-G, GOR132-G, and StHs6/80-G from the Max-Planck-Institut für Chemie-Dingwell (MPI-DING) collection (Jochum et al., 2005; Jochum et al., 2006).

Llao Rock tephra reference material analyses from Foit and Mehringer (2016) were conducted at the GeoAnalytical Laboratory located in the Geology Department (School of the Environment) at Washington State University, WA, USA, using Cameca Camebax and JOEL JXA 8500F electron microprobes. Both instruments were operated with a 8-µm beam diameter, 12 nA beam current, and 15kV accelerating voltage.

Tephra reference material analyses from Pyne-O'Donnell et al. (2012) were conducted at the Electron Microprobe Laboratory, University of Alberta using a JEOL 8900 electron microprobe with a 10-µm beam diameter, 6-nA beam current and 15-keV accelerating voltage. Where analyses of smaller shards required a 5-µm beam diameter, a Cameca SX100 was employed with a reduced beam current of 3-nA and measurement of SiO_2 by energy-dispersive spectrometry.

Kamchatka tephra reference material analyses from Kyle et al. (2011) were conducted at New Mexico Tech, Socorro, NM, USA, using a Cameca SX-100 electron microprobe with a 10 nA beam current and 15-kV accelerating voltage. Peak counts were 20 seconds for all elements, except Na, Cl, S, and F which were counted for 40, 40, 60, and 100 seconds, respectively. Depending on the glass shard sizes, a 5, 10, 15, 20, or 25 µm-diameter beam was used.

Aleutian tephra reference material analyses from Carson et al. (2002) were conducted at the University of Wisconsin-Madison, WI, USA, using a Cameca SX-51 electron microprobe with a 7-10-µm beam diameter, 6 nA Faraday beam current, and 15-keV accelerating voltage.

Each analysis represents a single tephra grain.

References in the "Microprobe operating conditions note" only:

Jochum, K.P., Nohl, U., Herwig, K., Lammel, E., Stoll, B., and Hofmann, A.W., 2005, GeoReM: A new geochemical database for reference materials and isotopic standards: Geostandards and Geoanalytical Research, v. 29, p. 333–338, doi:https://doi.org/10.1111/j.1751-908X.2005.tb00904.x.

Jochum, K.P., et al., 2006, MPI-DING reference glasses for in situ microanalysis: New reference values for element concentrations and isotope ratios: Geochemistry Geophysics Geosystems, v. 7, Q02008, doi:https://doi.org/10.1029/2005GC001060.

*Glass shard data normalized to water-free compositions (100 wt %) and displayed alongside original analytical totals.

† N.D. = no data.